nature microbiology

LETTERS

https://doi.org/10.1038/s41564-020-00799-3

Check for updates

β-Barrels covalently link peptidoglycan and the outer membrane in the α-proteobacterium *Brucella abortus*

Pierre Godessart[1], Adélie Lannoy[1], Marc Dieu[2], Sander E. Van der Verren[3,4], Patrice Soumillion[5], Jean-François Collet[6,7], Han Remaut[3,4], Patricia Renard[2,8] and Xavier De Bolle[1]✉

Gram-negative bacteria are surrounded by a cell envelope that comprises an outer membrane (OM) and an inner membrane that, together, delimit the periplasmic space, which contains the peptidoglycan (PG) sacculus. Covalent anchoring of the OM to the PG is crucial for envelope integrity in *Escherichia coli*. When the OM is not attached to the PG, the OM forms blebs and detaches from the cell. The Braun lipoprotein Lpp[1] covalently attaches OM to the PG but is present in only a small number of γ-proteobacteria; the mechanism of OM–PG attachment in other species is unclear. Here, we report that the OM is attached to PG by covalent cross-links between the N termini of integral OM β-barrel-shaped proteins (OMPs) and the peptide stems of PG in the α-proteobacteria *Brucella abortus* and *Agrobacterium tumefaciens*. Cross-linking is catalysed by L,D-transpeptidases and attached OMPs have a conserved alanyl-aspartyl motif at their N terminus. Mutation of the aspartate in this motif prevents OMP cross-linking and results in OM membrane instability. The alanyl-aspartyl motif is conserved in OMPs from Rhizobiales; it is therefore feasible that OMP–PG cross-links are widespread in α-proteobacteria.

The envelope of Gram-negative bacteria is a complex, macromolecular structure that is essential for growth and survival. Since the first observation of its multilayered structure in the 1960s, major efforts have been made to both investigate its unique structural features and unravel the mechanisms that govern its assembly. After decades of intense scrutiny, we now have a reasonably good understanding of the molecular processes that assemble and maintain the envelope of the model organism *E. coli*, although crucial questions remain unresolved. Knowledge gained in *E. coli* can be applied, at least partially, to other less-studied organisms. However, *E. coli* presents some features that are found only in Enterobacteriaceae. For example, the Braun's lipoprotein Lpp is one of the hallmarks of the *E. coli* envelope. With a presence of ~1,000,000 copies per cell, Lpp is numerically the most abundant *E. coli* protein[1]. Lpp has a crucial role in the cell envelope, because it is anchored to the OM by a lipid moiety at its N terminus and attached to the PG through its C-terminal lysine. Lpp provides the only known covalent connection between the OM and the PG. This anchorage has major implications; when absent, the OM pulls away from the cell and forms blebs[2]. Although other envelope proteins, such as the lipoprotein Pal and the OM protein (OMP) OmpA, bind non-covalently to PG, they cannot fully compensate for the loss of Lpp. Further highlighting its importance in *E. coli*, Lpp has recently been shown to also dictate the size of the periplasm[3,4]—the intermembrane distance increases when Lpp becomes longer. Thus, Lpp is a key component of the *E. coli* cell envelope. Given the important function of Lpp in *E. coli*, as well as its role in pathogenesis[5], we were intrigued by the absence of this protein in most Gram-negative bacteria, raising the possibility that other OM–PG covalent tethers remain unidentified. We investigated this prospect using the α-proteobacterium *B. abortus*—which is a Gram-negative intracellular pathogen, and is the aetiological agent of brucellosis, a zoonosis that causes major social and economic impacts worldwide[6].

To investigate whether OM proteins are covalently attached to PG in *B. abortus*, PG sacculi were purified and digested with either lysozyme (cleaving the β-1-4 bond between the *N*-acetylglucosamine (NAG) and *N*-acetylmuramic acid (NAM) residues) or an amidase (cleaving the amide bond between NAM and the L-alanine residue of the peptide stem), while the potentially linked proteins were digested with trypsin either alone or in combination with chymotrypsin. The resulting fragments were then analysed using liquid chromatography coupled with tandem mass spectrometry (LC–MS/MS). Out of 66 proteins identified, the most predominant proteins (in terms of spectra per protein) were predicted to be located in the OM (Fig. 1a). We found hybrid peptides between the *meso*-diaminopimelic acid (mDAP) residue from the peptide stems and the N termini of seven different proteins (Fig. 1b). All of the proteins are predicted to have a β-barrel-like structure and all except for one are OMPs. In the lysozyme-digested condition, we found that the oxonium ions corresponded to the NAG fragmentation (Extended Data Fig. 1a), therefore confirming the glycosylated nature of the hybrid fragments[7]. Supporting these data, when lysozyme-digested PG fragments were analysed using sodium dodecyl sulphate–polyacrylamide gel electrophoresis (SDS–PAGE), released Omp2b and Omp25 could be detected using immunoblotting (Extended Data Fig. 2).

Our data above indicate that OMPs are covalently attached to the PG in *B. abortus* (Fig. 1b). In *E. coli*, three L,D-transpeptidases (Ldts) catalyse the attachment of Lpp to the PG[8]. These enzymes use a cysteine-based enzymatic mechanism[9] to covalently link the C-terminal lysine residue of Lpp to the mDAP[10]. This prompted us to search for *B. abortus* Ldts. Analysis of the *B. abortus* genome

[1]Research Unit in Microorganisms Biology (URBM), Department of Biology, Namur Research Institute for Life Sciences (NARILIS), Namur, Belgium. [2]MaSUN, Mass Spectrometry Facility, University of Namur, Namur, Belgium. [3]Structural & Molecular Microbiology, VIB-VUB Centre for Structural Biology, Brussels, Belgium. [4]Structural Biology Brussels, Vrije Universiteit Brussel, Brussels, Belgium. [5]LIBST, UCLouvain, Louvain-la-Neuve, Belgium. [6]de Duve Institute, Université Catholique de Louvain, Brussels, Belgium. [7]WELBIO, Brussels, Belgium. [8]Laboratory of Biochemistry and Cell Biology (URBC), Department of Biology, Namur Research Institute for Life Sciences (NARILIS), Namur, Belgium. ✉e-mail: xavier.debolle@unamur.be

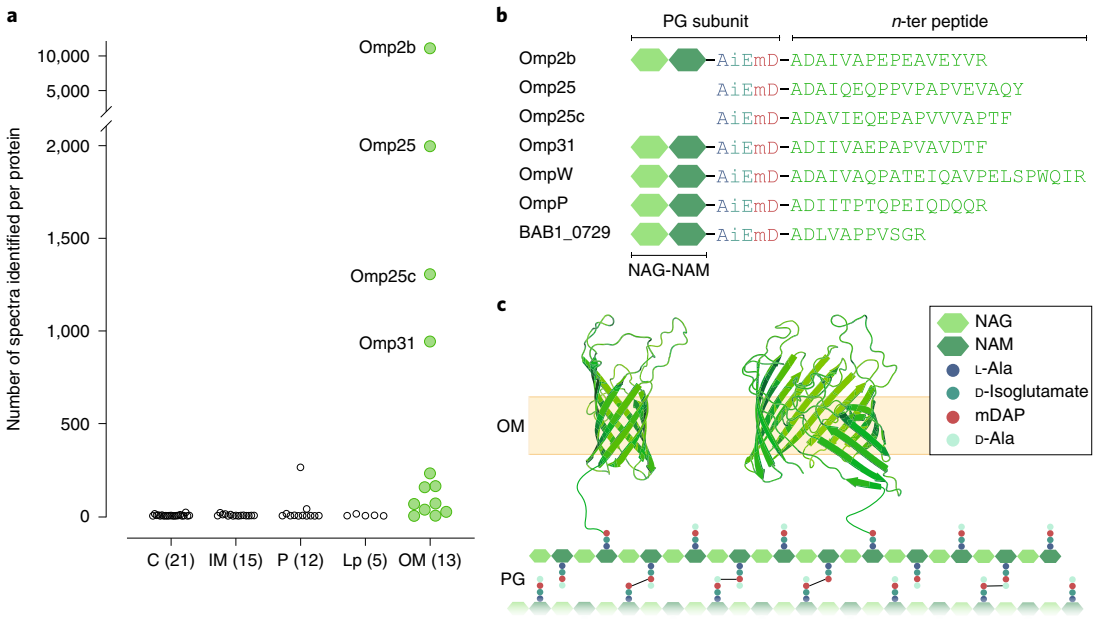

Fig. 1 | Multiple OM proteins are bound to PG. a, Classification of the 66 proteins purified with PG and identified in MS according to the number of spectra per protein and their predicted subcellular localization. Four proteins, which are all predicted to be β-barrels, were prevalent. The numbers in brackets correspond to the number of proteins predicted per subcellular localization. C, cytoplasmic; IM, inner membrane; Lp, lipoprotein; P, periplasmic. **b**, PG-linked identified proteins and their corresponding sequenced fragments at the N terminus of mature forms (*n*-ter). Proteins identified in lysozyme-treated samples were linked to the disaccharide NAG-NAM (Supplementary Fig. 1a). iE, isoglutamate; mD, mDAP. **c**, Model of OMPs linked through their N-terminal amino group to the mDAP of the PG. The 3D structures of the proteins were predicted using I-Tasser[45–47] and displayed with PyMol v.2.0, and represent Omp25 (left) and Omp2b (right).

revealed that it encodes eight proteins with sequence homology to *E. coli* Ldts. These putative Ldt genes were named *ldt1* to *ldt8* (Supplementary Table 3). To test whether these Ldts were able to covalently link OMPs to the PG, the coding sequences of these enzymes were expressed separately in *E. coli* cells also producing *B. abortus* Omp25. We then purified the PG of these *E. coli* strains and digested it with lysozyme. Omp25 was found attached to the PG only in cells expressing Ldt1, Ldt2 and Ldt4 (Fig. 2a). These three Ldts have a lipobox, being the only putative lipoproteins among the eight Ldts, and also form a monophyletic group (Extended Data Fig. 3).

Next, we deleted the eight identified Ldts either separately or in combination to assess their roles in OMP–PG attachment in *B. abortus*. We used the attachment of Omp2b and Omp25 to PG in *B. abortus* as a readout (Extended Data Fig. 4). Increased proportions of free OMPs were observed in the lysozyme-treated samples generated from cells lacking Ldt4, either alone or in combination with Ldt1 or Ldt2 (Fig. 2b and Extended Data Fig. 4). Complementation of both Δ*ldt4* and Δ*ldt1,2,4* strains with the *ldt4* gene increased the PG-bound protein forms and led to decreased pools of free Omp25 and Omp2b (Fig. 2b). By contrast, deletion of *ldt1* and *ldt2* had no impact. These results led us to conclude that Ldt4 is the main Ldt involved in OMP tethering to the PG in *B. abortus*. A fraction of OMPs remained linked in all of the mutants, indicating that at least one other unidentified enzyme might anchor OMPs to PG.

Brucella spp. release OM vesicles containing OM material[11]. We therefore hypothesized that altered OM–PG interactions might increase the production of OM vesicles under stress conditions. We exposed the wild-type (WT), Δ*ldt4* and Δ*ldt1,2,4* strains to heat stress. Whereas the WT strain released only small amounts of Omp25 at 60 °C, the deletion strains released detectable levels of Omp25 at 50 °C (Fig. 2c). We observed that Ldt1 and Ldt2 had a bigger impact on the envelope integrity when deleted in combination with the Ldt4 (Extended Data Fig. 5c). After heat stress, large OM blebs were observed for the Δ*ldt1,2,4* strain in cryo-electron microscopy (cryo-EM; Fig. 2d), consistent with the release of Omp25 in the culture supernatant. No change in periplasm size was observed between the WT and Δ*ldt1,2,4* strains (Extended Data Fig. 5a,b) in these conditions, suggesting that the remaining links between OM and PG preserve the global envelope structure. In agreement with this hypothesis, the Δ*ldt1,2,4* strain remained as infectious as the WT in murine macrophage infection assays (Extended Data Fig. 6). Together, these data indicate that, although the OM structure is not visibly affected under normal growth conditions, it is more sensitive to heat stress.

In *B. abortus*, all mature PG-bound OMPs begin with an alanyl-aspartyl motif that is conserved in other Rhizobiales (Fig. 3a). We next investigated the role of the aspartate residue in anchoring Omp25 and Omp2b to the PG. We replaced the *omp25* or *omp2b* genes with an allele in which the conserved aspartate 2 was substituted with an alanine residue, therefore generating two single mutants encoding Omp25^{D2A} or Omp2b^{D2A}. Although both proteins were still exported to the OM (Extended Data Fig. 7), they were no longer attached to the PG (Fig. 3b). The aspartate residue is therefore crucial for anchoring these OMPs to the PG. In the absence of the Omp25 linkage, a higher proportion of Omp2b was linked to the PG and conversely. On the basis of phase-contrast microscopy, the mutation of Omp25 or Omp2b alone had no phenotypical effect. However, the combination of both mutations led to a higher proportion of rounder cells compared with the WT (Extended Data Fig. 8a). The double mutant carrying Omp25^{D2A} and Omp2b^{D2A} (Omp25-2b^{D2A}) also showed the release of small blebs under normal growth conditions in EM (Fig. 3c,d). Furthermore, Omp25 could be detected in the supernatant of an Omp25-2b^{D2A} mutant suspension (Extended Data Fig. 8b), suggesting that there is increased blebbing in this strain. Similar to the Δ*ldt1,2,4* mutant, the Omp25^{D2A} strain also released OM material at a lower temperature compared with

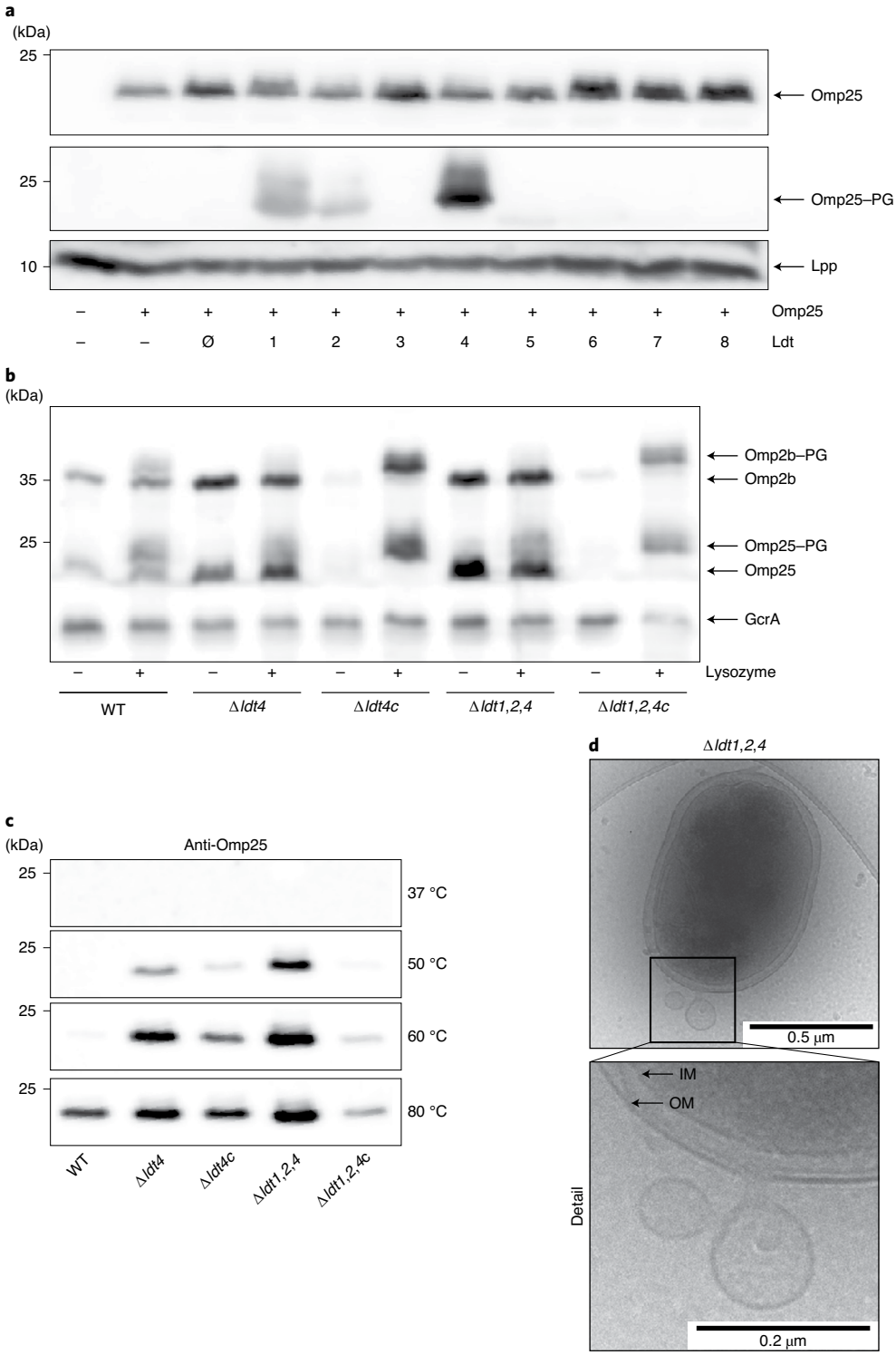

Fig. 2 | Ldts are involved in OMP-PG linkage and envelope stability. a, Coexpression of Omp25 and Ldts from *B. abortus* in *E. coli*. Omp25 was detected using western blot analysis of the cell lysates (top). When PG was isolated, Omp25 was detected only when coexpressed with *ldt1*, *ldt2* and *ldt4*, suggesting an anchorage of Omp25 to the *E. coli* PG (middle). Lpp was used as a loading control for PG (bottom). 'Ø' refers to the empty vector (without the *omp25* gene). **b**, The effect of deleting and complementing *ldt4* alone or in combination with *ldt1* and *ldt2* in *B. abortus*. A decrease in the bound forms of Omp25 and Omp2b and an increase in the free forms were observed in the deletion strains. Complementation with *ldt4* (Δ*ldt4c* and Δ*ldt1,2,4c*) led, in both cases, to a strong increase in the bound form with a depletion of the free form. GcrA was used as the loading control. **c**, Heat-stressed Δ*ldt4* and Δ*ldt1,2,4* strains release Omp25 at a lower temperature compared with the WT. Omp25 was detected using western blot analysis of the culture supernatants. Complementation strains have a partially restored phenotype. **d**, Cryo-EM observations of the Δ*ldt1,2,4* strain heat-stressed at 60 °C. The strain exhibits formation of blebs along the OM, supporting the release of Omp25. Scale bars, 0.5 µm (top) and 0.2 µm (bottom). For **a**–**d**, data are representative of experiments from three biologically independent replicates.

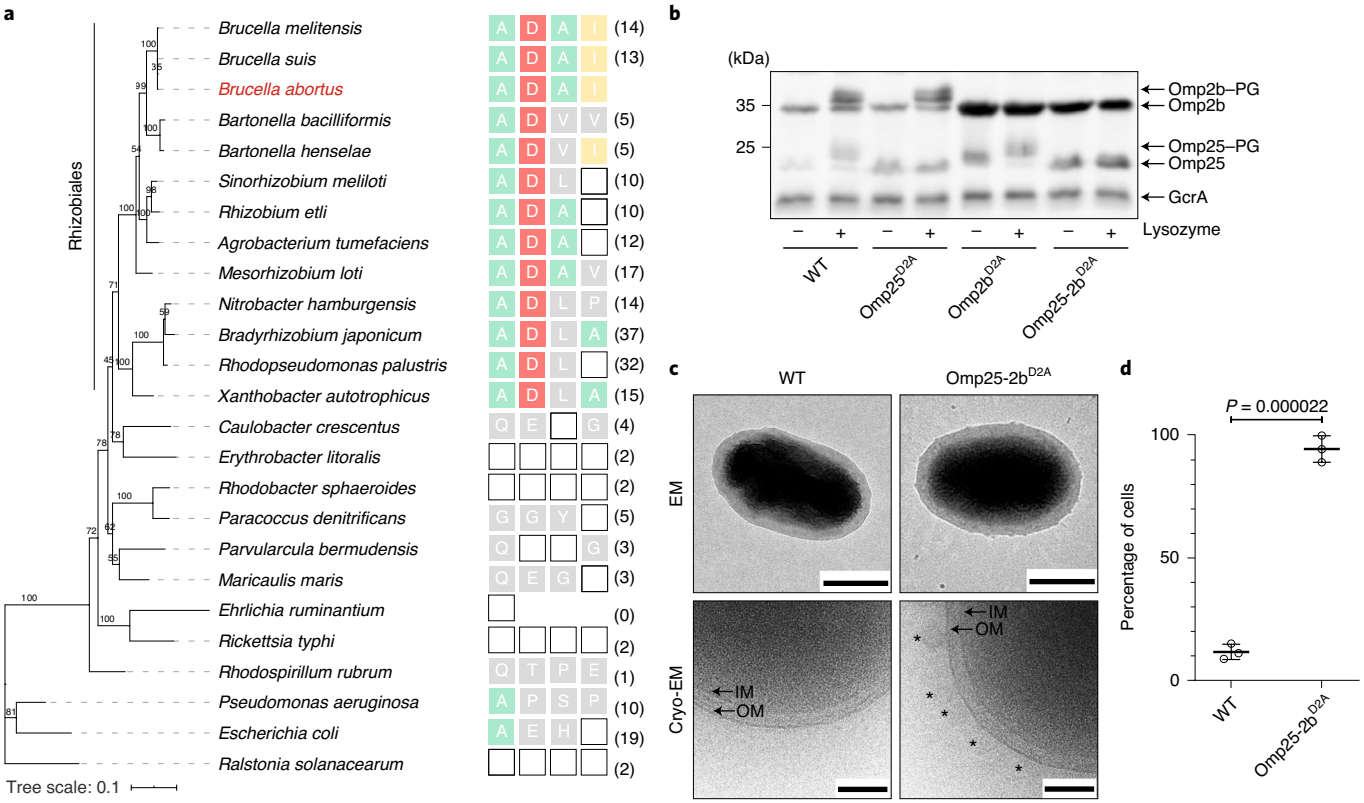

Fig. 3 | Aspartate 2 is crucial for the OMP anchorage to PG. a, Comparison between the first four amino acid consensus of *B. abortus* OMPs and their homologues found in α-proteobacteria. The phylogeny was inferred from the 16S and 23S RNA and bootstrap values are represented. The two first residues are conserved across Rhizobiales. The numbers in brackets represent the total number of homologues found in the listed organisms. An empty square indicates that there is no consensus sequence. **b**, Mutation of the Omp25 or Omp2b aspartate 2 into an alanine (D2A) abolished their linkage to PG, whereas an increased free form of Omp2b or Omp25, respectively, was concomitantly observed. GcrA was used as the loading control. The representative western blot was consistently observed over three biologically independent replicates. **c**, Electron microscopy (top) and cryo-EM (bottom) analysis of the WT and the Omp25-2b^{D2A} strains. The mutant strain shows an envelope instability with small blebs originating from the OM. The asterisks indicate blebs, which were consistently observed over three biologically independent replicates. Scale bars, 0.5 µm (top) and 0.1 µm (bottom). **d**, The Omp25-2b^{D2A} strain has a significantly higher proportion of bacterial cells that have at least one bleb detected on its envelope in EM. $n = 101$ for WT and $n = 111$ for Omp25-2b^{D2A} strains over three biologically independent experiments. Statistical significance was determined using unpaired two-tailed *t*-tests with the Holm–Sidak method. Data are mean ± s.d.

the WT. In line with the results above, the Omp25-2b^{D2A} mutant showed no reduced infectivity in macrophage infection assays, despite the altered structure of its envelope (Extended Data Fig. 6).

The alanyl-aspartyl motif is conserved in many mature OMPs homologues in several Rhizobiales, raising the interesting possibility that the anchorage described above is conserved in this bacterial clade. To assess this hypothesis, the PG from the plant pathogen *A. tumefaciens* was isolated to identify PG-bound OMPs. We found two proteins that are homologous to Omp2b and Omp25, named RopA1/A2 and RopB, respectively, that bind covalently to the mDAP of the PG through their N terminus (Extended Data Fig. 9). This suggests that a similar organization of OM–PG interactions is shared by the Rhizobiales, enabling the prediction of covalent anchorage of OMPs with an alanyl-aspartyl N terminus to the mDAP of the PG.

Our results address a long-standing question concerning the covalent attachment of the OM to the PG in bacteria that do not produce a Lpp homologue. Notably, we found that the identified linkage involves the N-terminal part of multiple integral OMPs. Depending on the OMP, this linker has a variable length and is thought to be flexible due to the absence of secondary structure. We also found that the formation of the covalent link is catalysed by L,D-transpeptidases, therefore revealing a new function for this large class of enzymes that is widely conserved in bacteria. In addition to being conserved in Rhizobiales, this mechanism is also found in other proteobacteria[12]. In the future, it will be important to characterize the envelope structure of other Gram-negative bacteria, as OM–PG tethering could be different in other clades. These investigations might result in leads for therapeutics to treat bacterial infections.

Methods

Plasmids and strains. *E. coli* DH10B, S17-1 and derivative strains were grown in Luria–Bertani (LB) medium at 37 °C under constant agitation. *B. abortus* 544 and derivative strains were grown in TSB-rich medium (3% Bacto Tryptic Soy Broth) at 37 °C under constant agitation. *A. tumefaciens* C58 was grown in 2YT-rich medium (1% yeast extract, 1.6% peptone, 0.5% NaCl) at 30 °C. When necessary, culture medium was supplemented with the appropriate antibiotics at the following concentrations: kanamycin, 10 µg ml^{-1} or 50 µg ml^{-1} for genomic or plasmidic resistance, respectively; chloramphenicol, 20 µg ml^{-1}; and nalidixic acid, 25 µg ml^{-1}.

Strain construction. A list of the strains, plasmids, open reading frames and primers used in this study is provided in Supplementary Tables 1–4, respectively. Deletion strains were constructed by allelic exchange with a pNPTS138 carrying a kanamycin resistance cassette and a sucrose sensitivity cassette as previously described[13]. For the expression of Ldts in *E. coli*, the Ldt sequences were amplified with 500 bp upstream and 100 bp downstream of the coding sequence and the amplicon was then inserted into a pNPTS138 restricted at the EcoRV site.

PG purification for MS. PG purification was performed using a modified version of a previously published method[14]. Bacteria were collected from exponential-phase culture by centrifugation (7,000*g* for 5 min at 4 °C), and then resuspended in lysis buffer (Tris-HCl 10 mM pH 7.5, NaCl 100 mM, DNase 100 µg ml^{-1} (Roche, 10104159001) and protease inhibitor cocktail EDTA-free (Roche, 11873580001)). Cells were then disrupted with 0.1 mm zirconia/silica beads (Biospec Products, 11079101z) in a Cell Disruptor Genie (Scientific Industries) at maximal amplitude (2,800 rotations per minute) for 60 min at 4 °C. Samples were then inactivated at 80 °C for 1 h. Envelopes were collected by centrifugation at 10,000*g* for 10 min at room temperature and resuspended in 5% SDS. The samples were boiled until the solution become translucent at 95 °C, 500 r.p.m. (Thermomixer, Eppendorf) and were then centrifuged (16,200*g* for 30 min at 14 °C). The samples were then resuspended in 5% SDS and boiled again for 30 min at 95 °C. This step was repeated five times to ensure that most of contaminant proteins were removed. The samples were then washed repeatedly with distilled water until SDS-free. PG pellets were resuspended in PBS and stored at −20 °C.

Proteomic analysis. PG was digested overnight with either lysozyme (Roche, 10006829, 10 µg for 45 µl of PG at ~1 mg ml^{-1}) or with the recombinant amidase Atl from *Staphylococcus aureus* (60 µg for 100 µl of a PG sample ±50 mg ml^{-1}), purified and used as described previously[15]. The samples were then reduced with dithiothreitol (10 mM at 37 °C for 45 min) and then alkylated with iodoacetamide (40 mM at 37 °C for 45 min) before protein digestion with trypsin (0.5 µg, Promega) overnight or trypsin overnight followed by treatment with chymotrypsin (0.25 µg, Promega) for 2 h for the amidase-treated samples. The digested samples were then analysed using nanoLC (UltiMate 3000, Thermo Fisher Scientific) coupled to electrospray MS/MS (maXis Impact UHR-TOF, Bruker). Peptides were separated by reverse-phase LC using a 75 µm × 250 mm column (Acclaim PepMap 100 C18). Mobile phase A was composed of 95% H_2O, 5% acetonitrile and 0.1% formic acid. Mobile phase B was composed of 80% acetonitrile, 20% H_2O and 0.1% formic acid. After injection of the peptides, the gradient started linearly from 5% B to 40% B in 220 min and from 40% B to 90% B in 10 min. The column was directly connected to a CaptiveSpray source (Bruker). In survey scans, MS spectra were acquired for 0.5 s in the *m*/*z* range of 400–2,200. The most intense peptides (2^+, 3^+ or 4^+ ions) were sequenced during a cycle time of 3 s. The collision-induced dissociation energy was automatically set according to the *m*/*z* ratio and the charge state of the precursor ion. To improve oxonium ion detection and glycopeptide sequencing, a second nanoLC–MS/MS analysis was performed using a basic stepping mode in MS/MS for which the collision energy was increased by 30% (ref. [7]) to half the sequencing time. The MaXis and Ultimate systems were controlled by Compass HyStar 3.2 (Bruker). Peak lists for all of the samples were created using DataAnalysis v.4.0 (Bruker) and saved as MGF files. Mascot v.2.4 (Matrix Science) and X! Tandem (The GPM; https://thegpm.org; version, CYCLONE 2010.12.01.1) were used as the search engine for protein identification. Enzyme specificity was set to trypsin or trypsin and chymotrypsin, and the maximum number of missed cleavages per peptide was set to one for trypsin alone or two when trypsin was used in combination with chymotrypsin. Carbamidomethyl (Cys), oxidation (Met), deamidation (Asn, Gln) for the amidase-treated samples and NAG(1)NAM(1) (478.179 Da) modification were variably enabled on alanines. The non-conventional amino acid mDAP (172.085 Da) was added to the amino acid configuration file from Mascot (Matrix Science). Mass tolerance for the monoisotopic peptide was 10 ppm and the MS/MS tolerance window was set to 0.05 Da. For protein identification, we used a custom-made database comprising the *B. melitensis* biovar *abortus* 2308 or *A. tumefaciens* C58 proteome downloaded from UniProt (July 2018 or June 2019, respectively) with the candidate protein modified sequences. The modified sequences consisted of a duplication of the sequence, a removal of the signal peptide to correspond to the mature proteins and the addition of the PG amino acids AEJ (where J is mDAP). The list of proteins with modified sequences is provided in Source Data Fig. 1 and Source Data Extended Data Fig. 9.

Scaffold v.4.8 (Proteome Software) was used to validate MS/MS-based peptide and protein identifications. Peptide identifications were accepted if they could be established at a probability of greater than 95% using the PeptideProphet algorithm[16] with Scaffold delta-mass correction. Protein identifications were accepted if they could be established at greater than 5.0% probability to achieve a false-detection rate of less than 1.0% and contained at least two identified peptides. Protein probabilities were assigned by the ProteinProphet algorithm[17]. Subcellular localization determination for the identified proteins was performed according to a decisional tree (Supplementary Fig. 1).

PG isolation for validation in *E. coli*. PG for western blot analysis was prepared according to a previously published method[18]. *E. coli* overnight cultures of 50 ml were normalized between them and centrifuged to recover bacteria (7,000*g* for 5 min at room temperature). The pellets were resuspended in 5% SDS and incubated at 95 °C, 500 r.p.m. (Thermomixer, Eppendorf) until the solution became translucent. PG was pelleted by centrifuging the samples at 16,200*g* for 30 min at 14 °C. The pellets were then washed by resuspension in distilled water, and the centrifugation steps described above were repeated until the sample was SDS-free. The pellets were resuspended in PBS and digested overnight with 2.5 U of mutanolysin (Sigma-Aldrich, M9901) per 50 µl of PG suspension.

PG isolation for validation in *B. abortus*. Exponential-phase cultures (optical density at 600 nm (OD_{600}) of 0.3–0.6) of *B. abortus* were normalized to an OD_{600} of 2 in 50 µl and inactivated for 1 h at 80 °C. Half of the sample was then digested overnight at 37 °C with lysozyme (8 µg). The digested and undigested samples were then treated with DNase I (10 µg, Roche) for 30 min at 37 °C. The sample volumes were then adjusted to 30 µl.

Western blot analysis. SDS-β-mercaptoethanol loading buffer, at final concentrations of 2% and 5%, was added (1:4 of final volume) before heating the samples at 95 °C for 10 min. Samples were loaded on 12% acrylamide gels. After migration, proteins were transferred in a semi-dry manner onto a nitrocellulose membrane (GE Healthcare Amersham Protran 0.45 NC) and then blocked in PBS supplemented with 0.05% Tween-20 (VWR) and 5% (w/v) milk (Nestlé, Foam topping) overnight at 4 °C on rollers. Before antibody incubation, the membranes were washed three times with PBS with 0.05% Tween-20. Membranes were incubated with primary antibodies (anti-Omp25 and anti-Omp2b, 1:200; anti-PG, 1:100; and anti-GcrA, 1:1,000; Supplementary Table 5) for 1 h followed by the corresponding secondary horseradish-peroxidase-coupled antibody (1:5,000, Supplementary Table 6). Both antibodies were diluted in PBS supplemented with 0.05% Tween-20 and 0.5% milk, and the membranes were washed as described after both incubations. The membranes were revealed using Clarity ECL Substrate (Bio-Rad) solutions and images were acquired using a GE Healthcare Amersham Imager 600. The specificity of anti-Omp25 and anti-Omp2b monoclonal antibodies was checked (Supplementary Fig. 2). Lpp was detected by immunoblot analysis using anti-Lpp antibodies (dilution, 1:10,000) produced from a rabbit (Eurogentec) immunized with the purified synthetized peptide KVDQLSNDVNAMRSDVQAAK from the middle part of the Lpp protein.

OM vesicle analysis. Exponential-phase bacteria were concentrated at an OD_{600} of 5 in 1 ml and washed twice in PBS, and then 200 µl of the sample was used for incubation at the different temperatures for 1 h. After incubation, bacteria were pelleted at 8,000*g* for 150 s and 100 µl of the supernatants were recovered and inactivated at 80 °C for 1 h. Then, 30 µl of the sample was added to 10 µl of 4× SDS-β-mercaptoethanol loading buffer and processed as described above for western blotting.

RAW 264.7 macrophage culture and infection. RAW 264.7 murine macrophages (ATCC) were cultured at 37 °C under 5% CO_2 in DMEM (GIBCO) supplemented with 10% decomplemented fetal bovine serum (GIBCO). For infections, RAW 264.7 macrophages were seeded in 24-well plates at a density of 10^5 cells per well and left overnight for growth and adhesion. The next day, *B. abortus* infectious doses were prepared in DMEM from exponential cultures (OD_{600} of 0.3–0.6) washed twice at a multiplicity of infection of 50. Bacteria and cells were centrifuged at 169*g* at 4 °C for 10 min and incubated until the appropriate time point at 37 °C, 5% CO_2. One hour after the beginning of infection, the culture medium was replaced with DMEM supplemented with 50 µg ml^{-1} of gentamycin to kill the remaining extracellular bacteria. One hour later, culture medium was changed again with fresh DMEM supplemented with 10 µg ml^{-1} of gentamycin. At the different time points (that is, 2 h, 5 h, 24 h and 48 h after infection), the cells were washed twice in PBS, and then lysed with PBS with 0.1% Triton X-100 for 10 min at 37 °C. Dilutions were then spotted (20 µl) onto TSB agar, incubated at 37 °C and colony-forming units were counted.

OMP labelling. Exponential-phase bacteria (OD_{600} of 0.3–0.6) were collected by centrifugation (8,000*g* for 150 s), washed twice in PBS then resuspended in undiluted hybridoma culture supernatant (Supplementary Table 5) and incubated at room temperature for 40 min on a wheel. Cells were then washed twice as described above and resuspended in the corresponding secondary antibody (Supplementary Table 6) diluted 500-fold in PBS and incubated at room temperature for 40 min on a wheel, protected from light. Cells were then washed as described above and resuspended in PBS for imaging.

Microscopy and analysis. Bacterial suspensions (2 µl) were spotted onto 1% agarose PBS pads for imaging. Images were acquired using a Nikon Eclipse Ti2 equipped with a phase-contrast objective Plan Apo λ DM100XK 1.45/0.13 PH3 and a Hamamatsu C13440-20CU ORCA-FLASH 4.0. Images were processed using FIJI v.2.0.0 (ref. [19]), a distribution of ImageJ. Look-up tables were adjusted to the best signal–noise ratio. Bacteria were detected and analysed using the ImageJ plugin MicrobeJ[20]. The parameters and pictures used for bacterial detection and measurements can be found at https://doi.org/10.6084/m9.figshare.12800795. Only bacteria with a maximal length of 1.4 µm were taken into account.

EM and cryo-EM analyses. Sample preparation was performed on the basis of a previously published protocol[21]. In brief, bacteria were collected in exponential phase by centrifugation (2 min at 8,000*g*), washed once with PBS and resuspended in paraformaldehyde (Merck) 4%. Fixation was performed at room temperature

for 1 h. Cells were then washed once in EM buffer (20 mM Tris-HCl pH 7.6, 50 mM glucose, 10 mM EDTA) before resuspension in EM buffer. Cell killing was confirmed before imaging. To assess the OM integrity of the Omp25-2b^{D2A} strain, biological triplicates of WT and mutant fixed bacteria were imaged using transmission EM, in the absence of negative staining reagents. All of the samples were prepared for EM by applying 5 µl sample to a non-glow discharged formvar copper 400 mesh grid (EMS) and washing once with 10 µl double-distilled H_2O. The prepared samples were imaged at ×15,000 nominal magnification (pixel size, 7.64 Å) using an in-house 120 kV JEM 1400+ (JEOL) microscope equipped with a LaB_6 filament and CMOS camera (TVIPS TemCam F-416). To assess periplasm size in the Δ*ldt1,2,4* strain and OM defects in the Omp25^{D2A} mutant, samples were additionally prepared for cryo-EM. Fixed bacteria were vitrified on glow-discharged Lacey carbon films on 300 mesh copper EM-grids (Agar-scientific). For each grid, 3 µl of sample was manually back-blotted and plunged into liquid ethane using a CP3 Cryoplunge (Gatan). For the Δ*ldt1,2,4* strain, images were acquired using a JEM-1400+ (JEOL) microscope. Images were obtained with a defocus of between −7 µm and −10 µm at ×25,000 nominal magnification, corresponding to a pixel size of 4.584 Å. For the Omp25^{D2A} mutant, images were acquired using a 300 kV JEOL CryoARM300 system (BECM, Brussels) equipped with an omega energy filter and a K3 detector (Gatan). Images were collected with a defocus range of −3 µm to −4 µm at a nominal magnification of ×25,000, corresponding to a pixel size of 2.01 Å. The detector was used in counting mode with a cumulative dose of 63.8 electrons per Å^2 spread over 60 frames. The images were motion-corrected and dose-weighted using MotionCor2.1 (ref. [22]) and defocus values were determined using ctffind4.1 (ref. [23]). Periplasmic space was measured using FIJI v.2.0.0 (ref. [19]), a distribution of ImageJ. In brief, membranes were manually delimited and distances between both membranes were computed at a 1 nm interval using a custom script (PeriSizer; https://doi.org/10.6084/m9.figshare.12806876) to produce the histogram. The pictures used for periplasm measurements are provided at https://doi.org/10.6084/m9.figshare.12806876.

Phylogeny analysis. For *ldt* phylogeny, *ldt* sequences from *B. abortus* were aligned with Clustal Omega v.1.2.4 (refs. [24–26]) without signal peptides (SignalP 4.1 Server[27]) and trimmed using TrimAI v.1.3 (ref. [28]). The best model was then determined using SMS[29], the phylogenetic analysis was performed using PhyML v.3.0 (refs. [30,31]) primed with BIONJ[32], and 100 bootstraps were performed. Visualization and tree annotation were performed using iTOL[33].

The tree of the alanyl-aspartyl motif conservation was constructed on the basis of the 16S and 23S RNA. Sequences were recovered for each organism listed from KEGG[34–36] and aligned separately using Clustal Omega v.1.2.4 (refs. [24–26]). The aligned sequences were then curated with Gblocks v.0.91b[37,38] and concatenated. The best model was then determined using jModeltest v.2.1 (ref. [39]). The phylogeny analysis was performed using PhyML v.3.0 (refs. [30,31]) primed with BIONJ[32], and 100 bootstraps were performed. Visualization and tree annotation were performed using iTOL[33].

Homology search and alignment. *B. abortus* OMPs homologues were searched using BLAST with the DELTA-BLAST[40–42] algorithm and an expected threshold of 10^{-5}. Signal peptides were then predicted using the SignalP 4.1 Server[27] and removed. Mature sequences were aligned using Clustal Omega[25] and viewed using Jalview v.2.10.5 (ref. [43]) to determine the consensus sequence. Protein sequences annotated as auto-transporter were manually removed.

Reporting Summary. Further information on research design is available in the Nature Research Reporting Summary linked to this article.

Data availability

All data are available at Figshare (https://doi.org/10.6084/m9.figshare.c.5087120) and raw MS data were deposited at the ProteomeXchange Consortium through the PRIDE[44] partner repository with the dataset identifier PXD019023. Source data are provided with this paper.

Code availability

The ImageJ script written for periplasm measurement is available on GitHub (https://github.com/pgodessa/PeriSizer).

Received: 16 December 2019; Accepted: 16 September 2020;
Published online: 2 November 2020

References

1. Asmar, A. T. & Collet, J. F. Lpp, the Braun lipoprotein, turns 50—major achievements and remaining issues. *FEMS Microbiol. Lett.* **365**, fny199 (2018).
2. Suzuki, H. et al. Murein-lipoprotein of *Escherichia coli*: a protein involved in the stabilization of bacterial cell envelope. *Mol. Gen. Genet.* **167**, 1–9 (1978).
3. Asmar, A. T. et al. Communication across the bacterial cell envelope depends on the size of the periplasm. *PLoS Biol.* **15**, e2004303 (2017).
4. Cohen, E. J., Ferreira, J. L., Ladinsky, M. S., Beeby, M. & Hughes, K. T. Nanoscale-length control of the flagellar driveshaft requires hitting the tethered outer membrane. *Science* **356**, 197–200 (2017).
5. Diao, J. et al. Peptidoglycan association of murein lipoprotein is required for KpsD-dependent group 2 capsular polysaccharide expression and serum resistance in a uropathogenic *Escherichia coli* Isolate. *mBio* **8**, e00603-17 (2017).
6. Moreno, E. & Moriyon, I. in *The Prokaryotes* Vol. 5 (Dworkin, M. et al.) Ch. 3.1.16, 315–456 (Springer, 2006).
7. Halim, A. et al. Assignment of saccharide identities through analysis of oxoniumion fragmentation profiles in LC–MS/MS of glycopeptides. *J. Proteome Res.* **13**, 6024–6032 (2014).
8. Magnet, S. et al. Identification of the L,D-transpeptidases responsible for attachment of the Braun lipoprotein to *Escherichia coli* peptidoglycan. *J. Bacteriol.* **189**, 3927–3931 (2007).
9. Mainardi, J. L. et al. A novel peptidoglycan cross-linking enzyme for a β-lactam-resistant transpeptidation pathway. *J. Biol. Chem.* **280**, 38146–38152 (2005).
10. Braun, V. & Bosch, V. Sequence of the murein-lipoprotein and the attachment site of the lipid. *Eur. J. Biochem.* **28**, 51–69 (1972).
11. Gamazo, C. & Moriyon, I. Release of outer membrane fragments by exponentially growing *Brucella melitensis* cells. *Infect. Immun.* **55**, 609–615 (1987).
12. Sandoz, K. M. et al. *Nat. Microbiol.* https://doi.org/10.1038/s41564-020-00798-4 (2020).
13. Deghelt, M. et al. G1-arrested newborn cells are the predominant infectious form of the pathogen *Brucella abortus*. *Nat. Commun.* **5**, 4366 (2014).
14. Moriyon, I. & Berman, D. T. Isolation, purification, and partial characterization of *Brucella abortus* matrix protein. *Infect. Immun.* **39**, 394–402 (1983).
15. Wheeler, R., Mesnage, S., Boneca, I. G., Hobbs, J. K. & Foster, S. J. Super-resolution microscopy reveals cell wall dynamics and peptidoglycan architecture in ovococcal bacteria. *Mol. Microbiol.* **82**, 1096–1109 (2011).
16. Keller, A., Nesvizhskii, A. I., Kolker, E. & Aebersold, R. Empirical statistical model to estimate the accuracy of peptide identifications made by MS/MS and database search. *Anal. Chem.* **74**, 5383–5392 (2012).
17. Nesvizhskii, A. I., Keller, A., Kolker, E. & Aebersold, R. A statistical model for identifying proteins by tandem mass spectrometry. *Anal. Chem.* **75**, 4646–4658 (2003).
18. Peters, K. et al. Copper inhibits peptidoglycan LD-transpeptidasessuppressing β-lactam resistance due to bypass of penicillin-binding proteins. *Proc. Natl Acad. Sci. USA* **115**, 10786–10791 (2018).
19. Schindelin, J. et al. Fiji: an open-source platform for biological-image analysis. *Nat. Methods* **9**, 676–682 (2012).
20. Ducret, A., Quardokus, E. M. & Brun, Y. V. MicrobeJ, a tool for high throughput bacterial cell detection and quantitative analysis. *Nat. Microbiol.* **1**, 16077 (2016).
21. Herrou, J. et al. Periplasmic protein EipA determines envelope stress resistance and virulence in *Brucella abortus*. *Mol. Microbiol.* **111**, 637–661 (2019).
22. Zheng, S. Q. et al. MotionCor2: anisotropic correction of beam-induced motion for improved cryo-electron microscopy. *Nat. Methods* **14**, 331–332 (2017).
23. Rohou, A. & Grigorieff, N. CTFFIND4: fast and accurate defocus estimation from electron micrographs. *J. Struct. Biol.* **192**, 216–221 (2015).
24. Goujon, M. et al. A new bioinformatics analysis tools framework at EMBL-EBI. *Nucleic Acids Res.* **38**, W695–W699 (2010).
25. Li, W. et al. The EMBL-EBI bioinformatics web and programmatic tools framework. *Nucleic Acids Res.* **43**, W580–W584 (2015).
26. McWilliam, H. et al. Analysis tool web services from the EMBL-EBI. *Nucleic Acids Res.* **41**, W597–W600 (2013).
27. Petersen, T. N., Brunak, S., von Heijne, G. & Nielsen, H. SignalP 4.0: discriminating signal peptides from transmembrane regions. *Nat. Methods* **8**, 785–786 (2011).
28. Capella-Gutierrez, S., Silla-Martinez, J. M. & Gabaldon, T. trimAl: a tool for automated alignment trimming in large-scale phylogenetic analyses. *Bioinformatics* **25**, 1972–1973 (2009).
29. Lefort, V., Longueville, J. E. & Gascuel, O. SMS: smart model selection in PhyML. *Mol. Biol. Evol.* **34**, 2422–2424 (2017).
30. Guindon, S. et al. New algorithms and methods to estimate maximum-likelihood phylogenies: assessing the performance of PhyML 3.0. *Syst. Biol.* **59**, 307–321 (2010).
31. Guindon, S. & Gascuel, O. A simple, fast, and accurate algorithm to estimate large phylogenies by maximum likelihood. *Syst. Biol.* **52**, 696–704 (2003).
32. Gascuel, O. BIONJ: an improved version of the NJ algorithm based on a simple model of sequence data. *Mol. Biol. Evol.* **14**, 685–695 (1997).
33. Letunic, I. & Bork, P. Interactive Tree Of Life (iTOL) v4: recent updates and new developments. *Nucleic Acids Res.* **47**, W256–W259 (2019).
34. Kanehisa, M. Toward understanding the origin and evolution of cellular organisms. *Protein Sci.* **28**, 1947–1951 (2019).
35. Kanehisa, M. & Goto, S. KEGG: Kyoto Encyclopedia of Genes and Genomes. *Nucleic Acids Res.* **28**, 27–30 (2000).

36. Kanehisa, M., Sato, Y., Furumichi, M., Morishima, K. & Tanabe, M. New approach for understanding genome variations in KEGG. *Nucleic Acids Res.* **47**, D590–D595 (2019).
37. Dereeper, A. et al. Phylogeny.fr: robust phylogenetic analysis for the non-specialist. *Nucleic Acids Res.* **36**, W465–W469 (2008).
38. Castresana, J. Selection of conserved blocks from multiple alignments for their use in phylogenetic analysis. *Mol. Biol. Evol.* **17**, 540–552 (2000).
39. Darriba, D., Taboada, G. L., Doallo, R. & Posada, D. jModelTest 2: more models, new heuristics and parallel computing. *Nat. Methods* **9**, 772 (2012).
40. Altschul, S. F. et al. Gapped BLAST and PSI-BLAST: a new generation of protein database search programs. *Nucleic Acids Res.* **25**, 3389–3402 (1997).
41. Boratyn, G. M. et al. Domain enhanced lookup time accelerated BLAST. *Biol. Direct* **7**, 12 (2012).
42. Schaffer, A. A. et al. Improving the accuracy of PSI-BLAST protein database searches with composition-based statistics and other refinements. *Nucleic Acids Res.* **29**, 2994–3005 (2001).
43. Waterhouse, A. M., Procter, J. B., Martin, D. M., Clamp, M. & Barton, G. J. Jalview version 2—a multiple sequence alignment editor and analysis workbench. *Bioinformatics* **25**, 1189–1191 (2009).
44. Perez-Riverol, Y. et al. The PRIDE database and related tools and resources in 2019: improving support for quantification data. *Nucleic Acids Res.* **47**, D442–D450 (2019).
45. Roy, A., Kucukural, A. & Zhang, Y. I-TASSER: a unified platform for automated protein structure and function prediction. *Nat. Protoc.* **5**, 725–738 (2010).
46. Yang, J. et al. The I-TASSER Suite: protein structure and function prediction. *Nat. Methods* **12**, 7–8 (2015).
47. Zhang, Y. I-TASSER server for protein 3D structure prediction. *BMC Bioinform.* **9**, 40 (2008).

Acknowledgements

We thank the members of the URBM for their discussions of the data; F. Tilquin and M. Waroquier for their logistic support; P. Cherry and C. Servais for their help with this project; V. Vassen for the *B. abortus* strains; C. Demazy for the MS sample preparation; I. Moriyon for his insights and ideas; S. Gillet for his help and knowledge regarding the script; S. Mesnage for sharing the amidase expression vector, M. Boutry for the *A. tumefaciens* strain and A. Asmar for the Lpp antibody; A. Cehovin and E. Lawarée for their reading of the manuscript; and staff at UNamur (https://www.unamur.be/) for financial and logistical support. P.G. was supported by a FRIA PhD fellowship. S.E.V.d.V. is supported by a FWO PhD fellowship. This work was funded by the Fédération Wallonie-Bruxelles (no. ARC 17/22-087), and by the FRS-FNRS (nos. PDR T.0060.15 and T.0058.20).

Author contributions

A.L. conducted PG extraction of *A. tumefaciens*. M.D. and P.R. performed the MS analysis. S.E.V.d.V. and H.R. performed the EM sample preparation and image acquisition. P.G. performed all of the other experiments. P.S. contributed to the initial conception of the work. P.G. and X.D.B. designed the experiments. P.G., X.D.B. and J.-F.C. wrote the manuscript.

Competing interests

The authors declare no competing interests.

Additional information

Extended data is available for this paper at https://doi.org/10.1038/s41564-020-00799-3.

Supplementary information is available for this paper at https://doi.org/10.1038/s41564-020-00799-3.

Correspondence and requests for materials should be addressed to X.D.

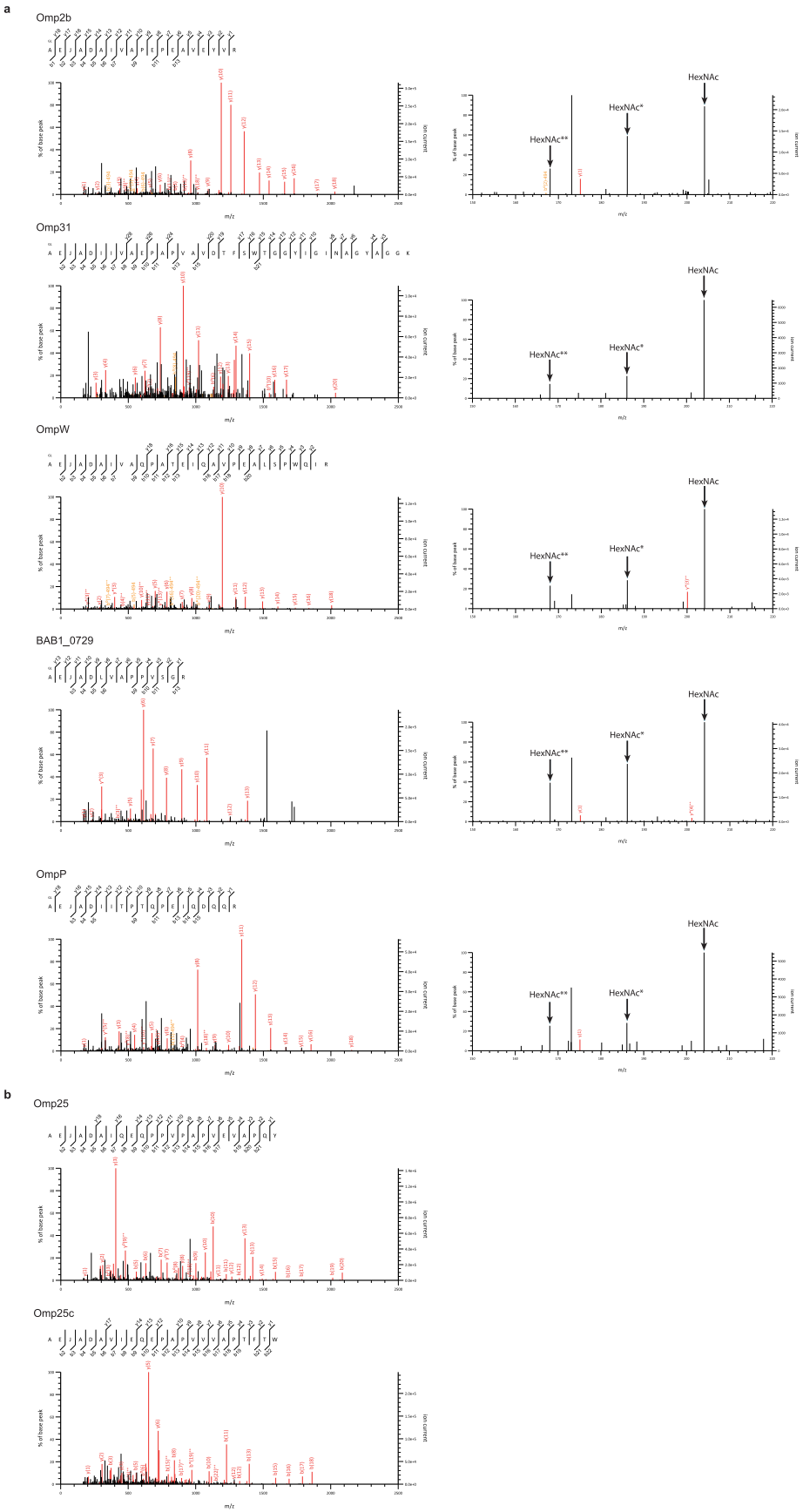

Extended Data Fig. 1 | See next page for caption.

Extended Data Fig. 1 | MS-MS fragmentation spectra of OMPs N-terminal peptides. a, Left panel, spectra obtained for Omp2b/31/W/P and BAB1_0729 from the analysis of lysozyme treated samples. PG disaccharide (NAG-NAM) modifications are indicated by « GL » on the sequence. Right panel, enlargement of the left spectra from 150 to 220 M/Z ratio. Glycosylation of peptides is confirmed by the presence of saccharide oxonium ions: HexNAc, $[C_8H_{14}NO_5]^+$ with a mass of 204.087; HexNAc*, HexNAc – H_2O, $[C_8H_{12}NO_4]^+$ with a mass of 186.076 and HexNAc**, HexNAc – 2 H_2O, $[C_8H_{10}NO_3]^+$ with a mass of 168.066. J corresponds to *m*DAP. **b**, Fragmentation spectra of the N-terminal peptides of Omp25 and 25c were obtained upon treatment with the amidase. The absence of glycosylation is due to the amidase activity.

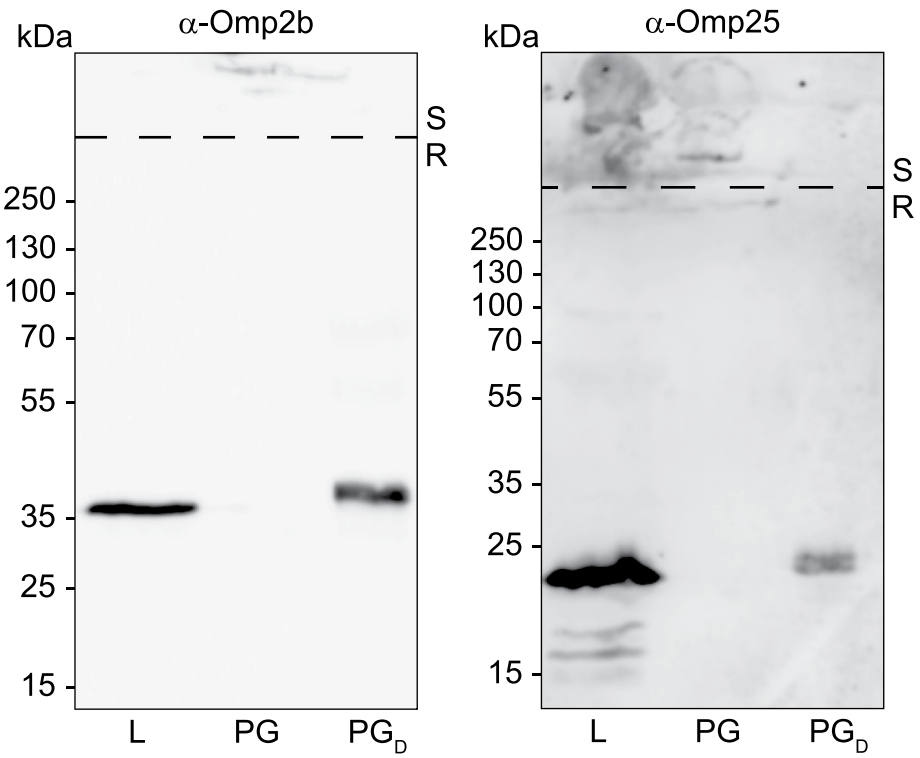

Extended Data Fig. 2 | Peptidoglycan binding induces a shift in the migration of Omp2b and Omp25 in Western blot. Upon digestion of purified *B. abortus* peptidoglycan with lysozyme, an apparent heavier weight is observed for Omp2b (left) and Omp25 (right) compared to the signal obtained with a lysate. A signal is observed in the stacking gel when the purified peptidoglycan is undigested. S, stacking gel; R, running gel; L, lysate; PG, peptidoglycan; PG_D, lysozyme-digested peptidoglycan. This experiment was not repeated. The shift induced by the PG binding is consistently observed in Fig. 3b.

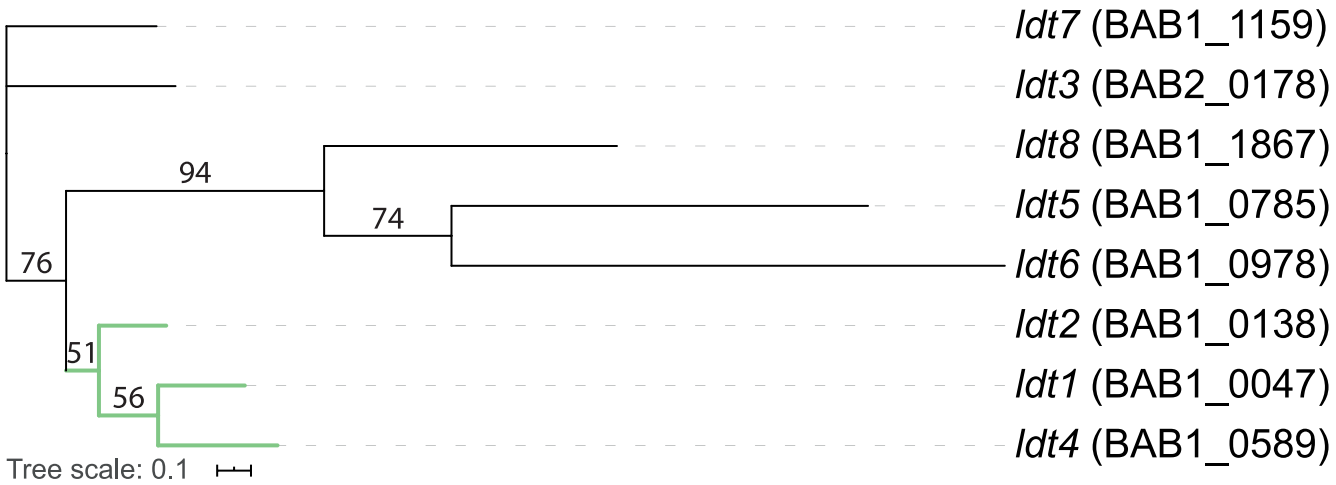

Extended Data Fig. 3 | Ldt1, Ldt2 and Ldt4 form a monophyletic cluster. Bootstrap values are represented above branches.

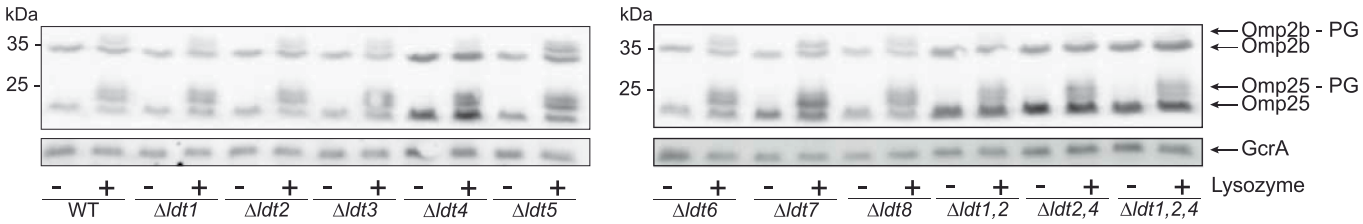

Extended Data Fig. 4 | Ldt4 has an impact on the linkage of Omp25 and Omp2b. Effect of the deletion of the eight *ldt* genes in *B. abortus*. The *ldt4* strain and derivatives (Δ*ldt1,4*, Δ*ldt2,4* and Δ*ldt1,2,4*) have a noticeable effect on the linkage of Omp25 and Omp2b. An increased signal corresponding to the free form of both OMPs is observed in these strains. GcrA was used as loading control.

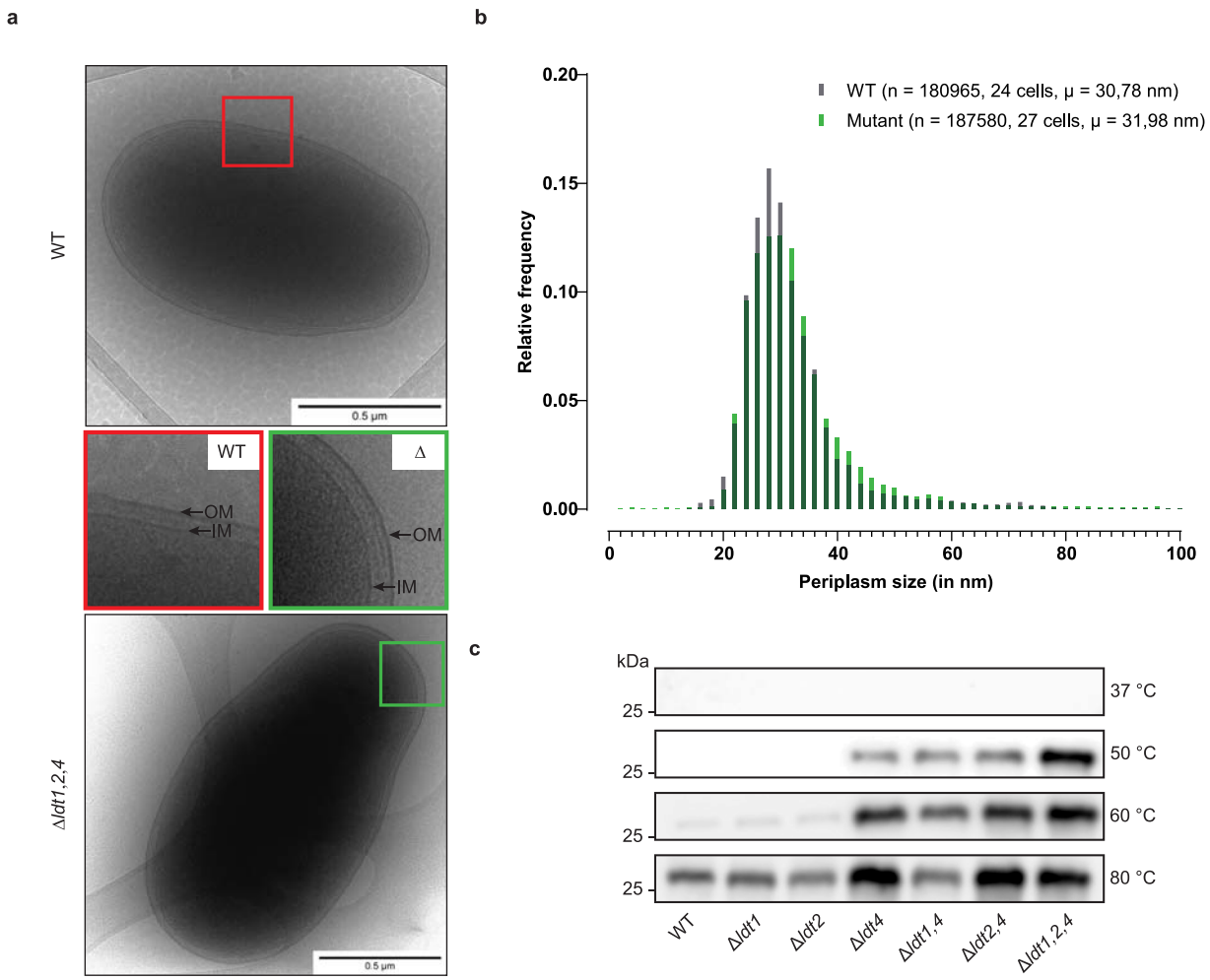

Extended Data Fig. 5 | Δ*ldt1,2,4* has no phenotype defect under normal growth conditions but is more sensitive to heat. a, Cryo-EM imaging of WT and Δ*ldt1,2,4* strains (« Δ »). No obvious defect can be seen between both strains. Enlarged portion delimited with coloured squares is shown in detail with the same colour code. Images were acquired with a defocus in the range of −7 to −10 µm. IM, inner membrane; OM, outer membrane. **b**, Comparison of the periplasm size distribution between the WT and the Δ*ldt1,2,4* strains. From 3 biological replicates, 24 cells were used and 180,965 measures were taken for the WT strain and 187,580 measures were obtained from 27 cells for the mutant. No significant difference was observed in the periplasm size between both strains. **c** Heat-stressed *ldt1* and *ldt2* strains have a WT-like phenotype for the release of Omp25 in culture supernatant. These results support the previous observations that Ldt1 and Ldt2 do not seem to have a major role in the OMP anchorage under normal growth conditions. This experiment is representative of 2 biologically independent replicates.

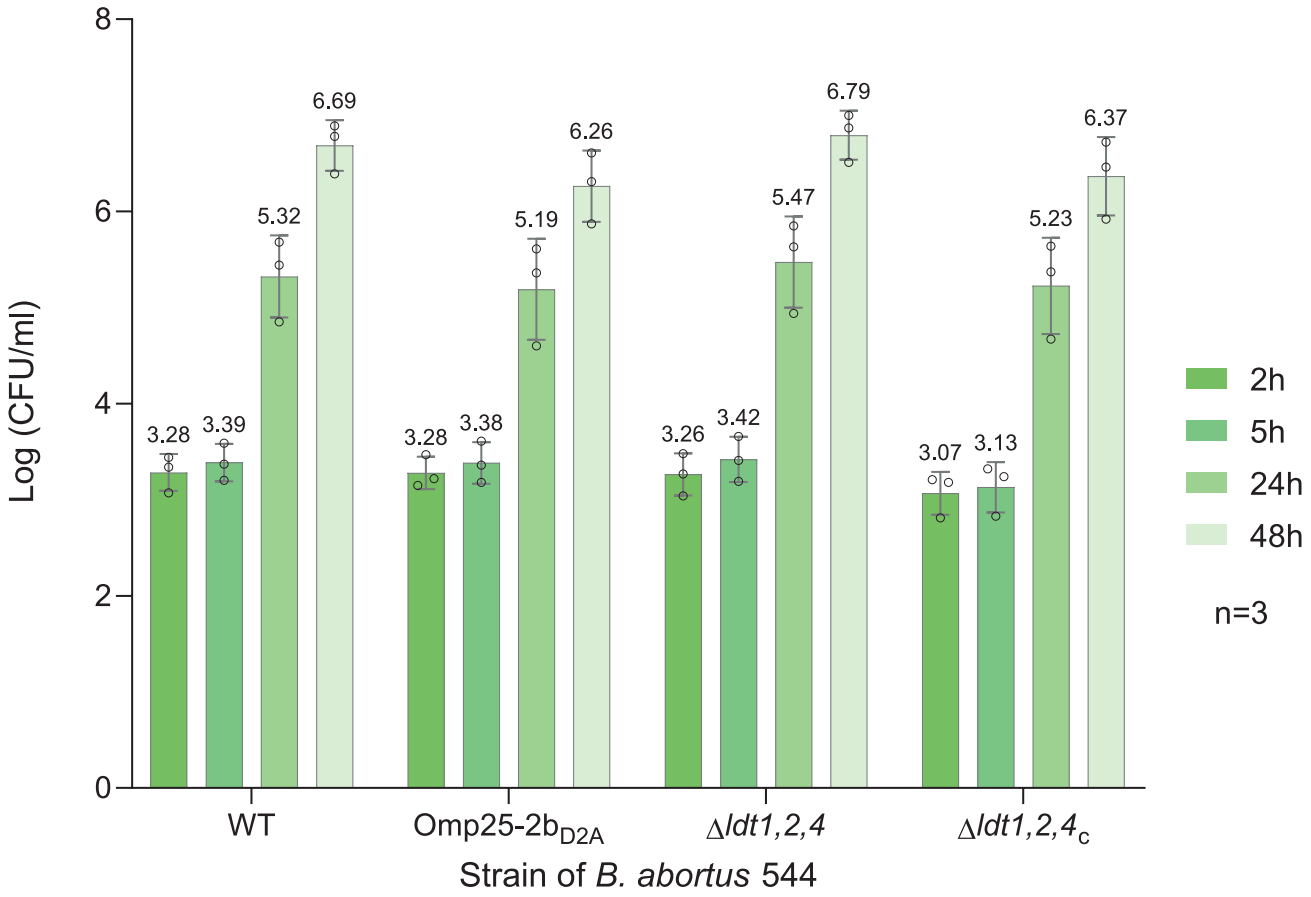

Extended Data Fig. 6 | Infectivity is not impacted in the Omp25-2b$_{D2A}$ or Δ*ldt1,2,4* strains. Murine RAW 264.7 macrophages were infected with *Brucella abortus* 544 WT, Omp25-2b$_{D2A}$, Δ*ldt1,2,4* or Δ*ldt1,2,4*c strains. Entry was assessed at 2 h post-infection (PI), survival at 5 h PI and replication at 24 h and 48 h PI. No difference was observed between the WT and the mutants. n = 3 biologically independent experiments, error bars, mean ± s.d.

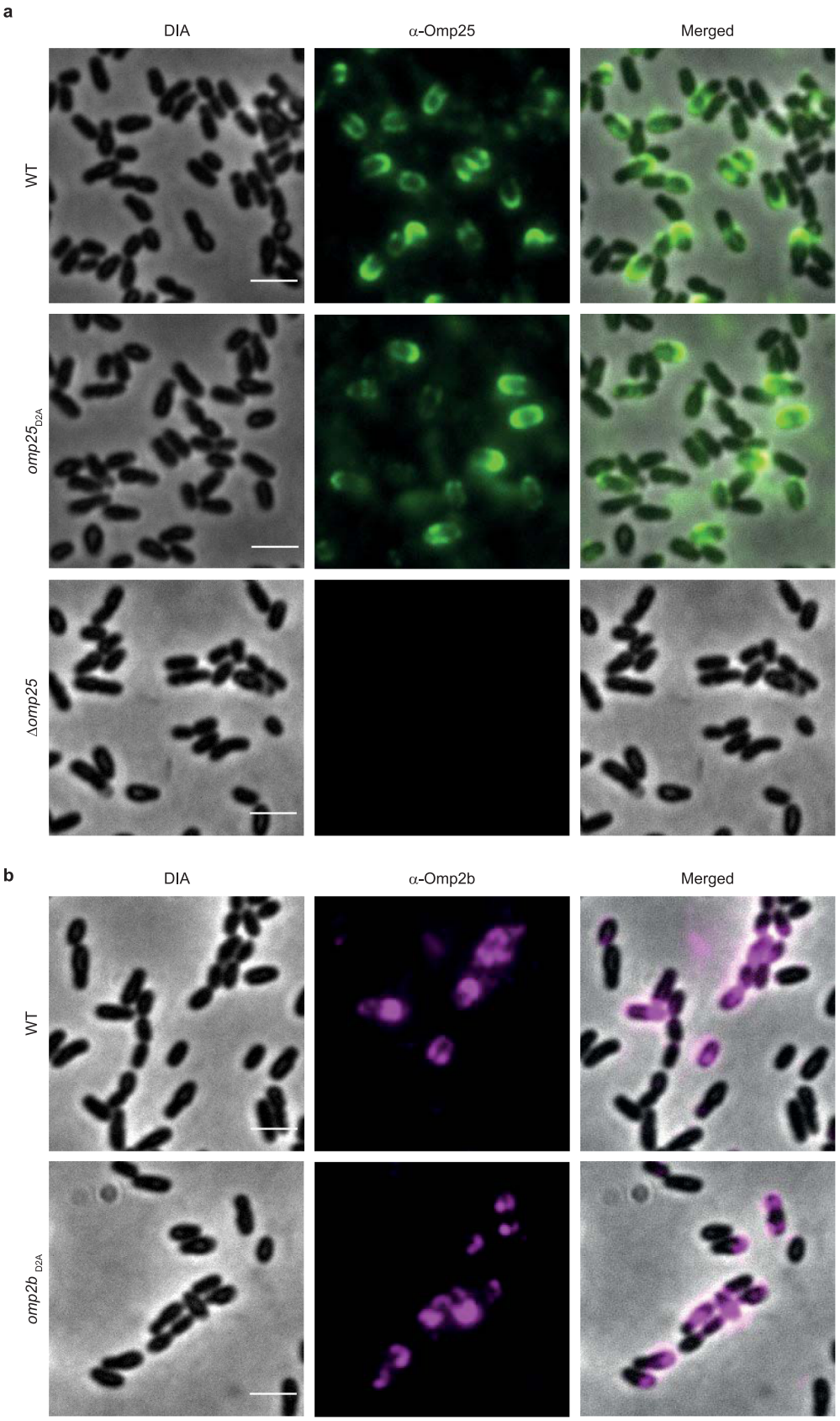

Extended Data Fig. 7 | Omp25$_{D2A\ and}$ Omp2b$_{D2A}$ are exported in the OM and detectable on the surface. a, Immunolabelling of Omp25 on the WT, *omp25*$_{D2A}$ and Δ*omp25* strains. A signal similar to the WT is observed in the *omp25*$_{D2A}$, suggesting a normal export of Omp25 and insertion at the OM. **b**, Immunolabelling of Omp2b on the WT and *omp2b*$_{D2A}$ strains. As for Omp25$_{D2A}$, Omp2b$_{D2A}$ is detectable on the bacterial surface. Scale bar is 2 µm.

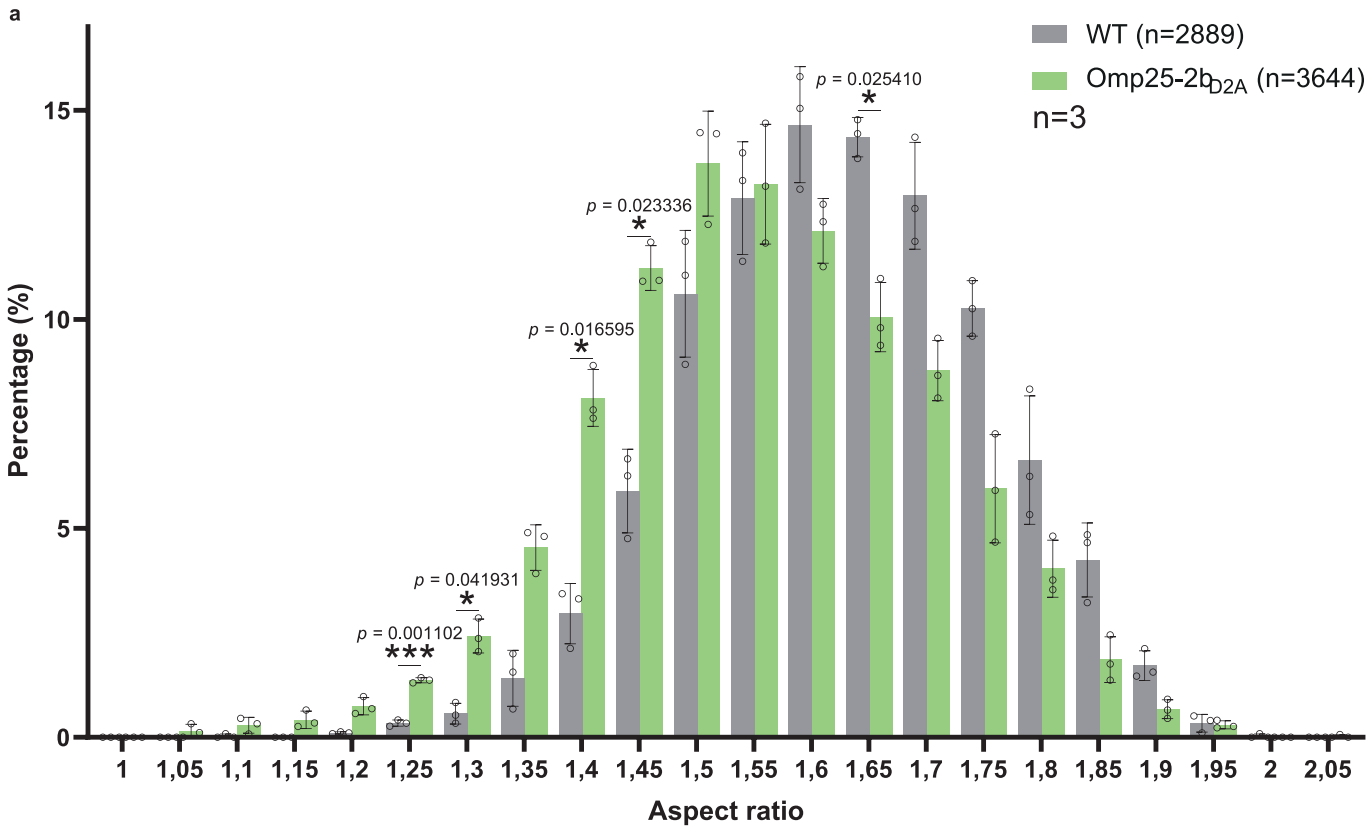

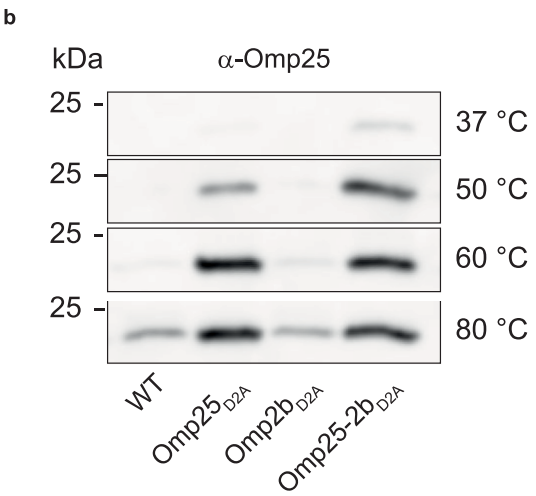

Extended Data Fig. 8 | Omp25-2b$_{D2A}$ strain has an envelope defect. a, The aspect ratio (major axis/minor axis) of both the WT and the Omp25-2b$_{D2A}$ strains was calculated and sorted according to their frequency. A shift of the distribution towards lower aspect ratios is observed for the mutant strains reflecting rounder cell shape. Statistical significance was determined using two-tailed unpaired *t*-tests with the Holm-Sidak method (with P<0.05), n = 2889 for WT and 3644 for Omp25-2b$_{D2A}$ strains cells examined over 3 independent experiments, error bars, mean ± s.d. **b**, Western blot analysis of the WT and D2A OMPs strains supernatants after incubation at different temperatures. The Omp25-2b$_{D2A}$ already release Omp25 at growth temperature indicating an outer-membrane instability.

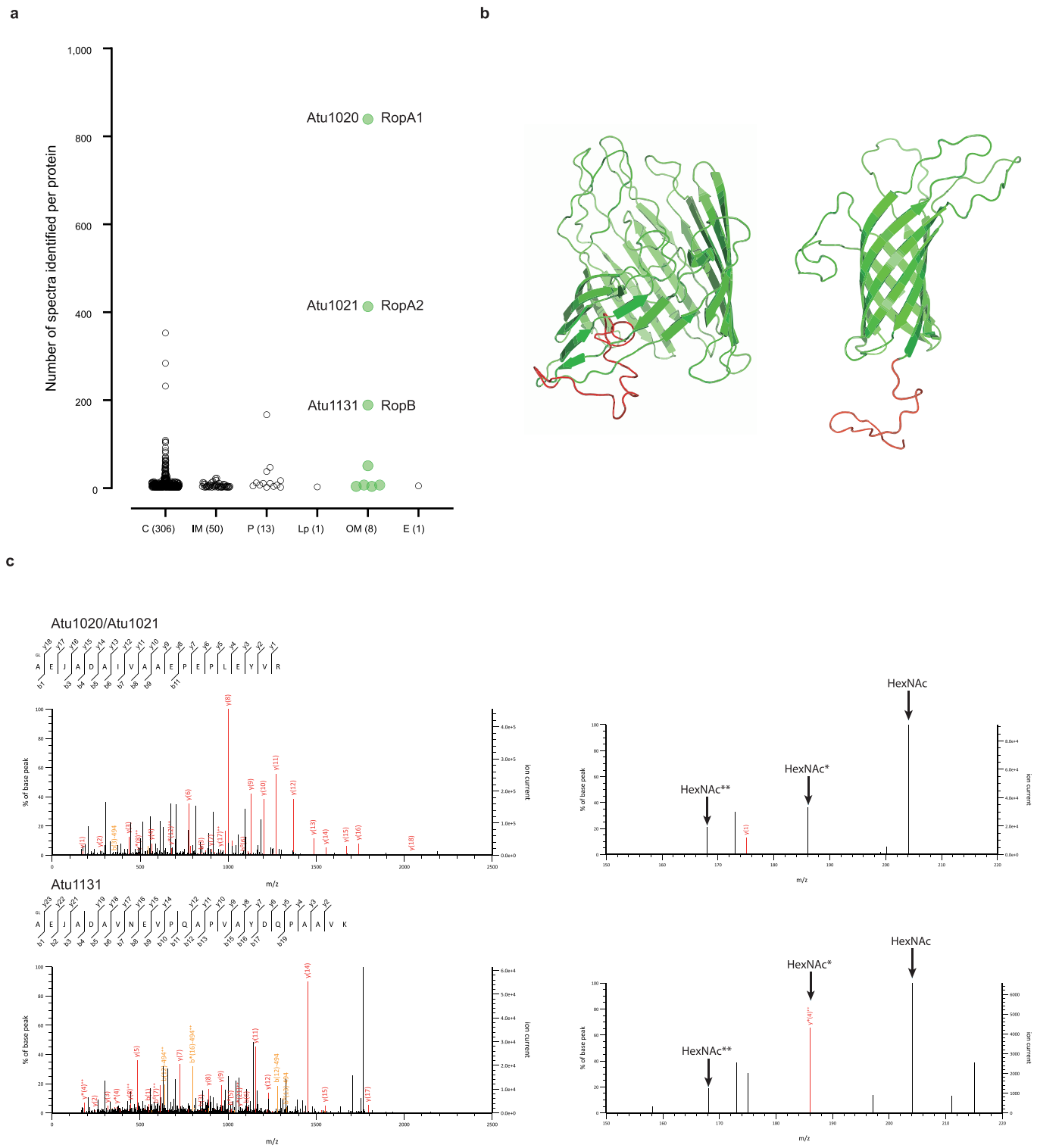

Extended Data Fig. 9 | *Agrobacterium tumefaciens* has a similar structure for the OMP-PG link to that of *B. abortus*. **a**, Classification of the 379 proteins isolated with PG and identified in mass spectrometry according to the number of spectra per protein and their subcellular localisation. Numbers in brackets correspond to the number of proteins predicted per subcellular localisation. C, Cytoplasmic; IM, Inner Membrane; P, Periplasmic; OM, Outer Membrane; E, extracellular. **b**, Three-dimensional predicted structure of the two predominant protein (Atu1020/1021, left; Atu1131, right) identified by mass spectrometry. Prediction were made using protein sequences without signal peptides and the I-TASSER server[44–46], and displayed with PyMol v.2.0. **c**, Spectra obtained for Atu1020/1021 and Atu1131 upon analysis of lysozyme treated samples. PG disaccharide (NAG-NAM) modifications are indicated by « GL » on the sequence. Glycosylation of peptides is confirmed by the presence of saccharide oxonium ions on the enlargement of the left spectra from 150 to 220 M/Z ratio. Glycosylation of peptides is confirmed by the presence of saccharide oxonium ions: HexNAc, $[C_8H_{14}NO_5]^+$ with a mass of 204.087; HexNAc*, HexNAc – H_2O, $[C_8H_{12}NO_4]^+$ with a mass of 186.076 and HexNAc**, HexNAc – 2 H_2O, $[C_8H_{10}NO_3]^+$ with a mass of 168.066. J corresponds to *m*DAP.

nature research

Corresponding author(s): Xavier De Bolle

Last updated by author(s): Aug 24, 2020

Reporting Summary

Nature Research wishes to improve the reproducibility of the work that we publish. This form provides structure for consistency and transparency in reporting. For further information on Nature Research policies, see Authors & Referees and the Editorial Policy Checklist.

Statistics

For all statistical analyses, confirm that the following items are present in the figure legend, table legend, main text, or Methods section.

n/a	Confirmed	
☐	☒	The exact sample size (*n*) for each experimental group/condition, given as a discrete number and unit of measurement
☐	☒	A statement on whether measurements were taken from distinct samples or whether the same sample was measured repeatedly
☐	☒	The statistical test(s) used AND whether they are one- or two-sided *Only common tests should be described solely by name; describe more complex techniques in the Methods section.*
☒	☐	A description of all covariates tested
☒	☐	A description of any assumptions or corrections, such as tests of normality and adjustment for multiple comparisons
☐	☒	A full description of the statistical parameters including central tendency (e.g. means) or other basic estimates (e.g. regression coefficient) AND variation (e.g. standard deviation) or associated estimates of uncertainty (e.g. confidence intervals)
☐	☒	For null hypothesis testing, the test statistic (e.g. *F*, *t*, *r*) with confidence intervals, effect sizes, degrees of freedom and *P* value noted *Give P values as exact values whenever suitable.*
☒	☐	For Bayesian analysis, information on the choice of priors and Markov chain Monte Carlo settings
☒	☐	For hierarchical and complex designs, identification of the appropriate level for tests and full reporting of outcomes
☒	☐	Estimates of effect sizes (e.g. Cohen's *d*, Pearson's *r*), indicating how they were calculated

Our web collection on statistics for biologists contains articles on many of the points above.

Software and code

Policy information about availability of computer code

Data collection	Mascot 2.4 and X! Tandem vCYCLONE 2010.12.01.1 were used for mass spectrometry
Data analysis	The following softwares were used for data analysis: Scaffold 4.8 (Proteome Software), Peptide Prophet Algorithm, Protein Prophet Algorithm, GraphPad Prism 8 (GraphPad Software), FIJI 2.0.0, a distribution of ImageJ, MicrobeJ plugin for ImageJ, MotionCor 2.1, Clustal Omega 1.2.4, SignalP 4.1, TrimAl 1.3, SMS, PhyML 3.0, BIONJ, iTOL, Gblocks 0.91b, jModeltest 2.1, DELTA-BLAST, Jalview 2.10.5

For manuscripts utilizing custom algorithms or software that are central to the research but not yet described in published literature, software must be made available to editors/reviewers. We strongly encourage code deposition in a community repository (e.g. GitHub). See the Nature Research guidelines for submitting code & software for further information.

Data

Policy information about availability of data

All manuscripts must include a data availability statement. This statement should provide the following information, where applicable:

- Accession codes, unique identifiers, or web links for publicly available datasets
- A list of figures that have associated raw data
- A description of any restrictions on data availability

All data are available at DOI: 10.6084/m9.figshare.c.5087120 and raw MS data were deposited at the to the ProteomeXchange Consortium via the PRIDE12 partner repository with the dataset identifier PXD019023 and DOI:10.6019/PXD019023. The ImageJ script written for periplasm measurement can be found on GitHub (https://github.com/pgodessa/PeriSizer).

Field-specific reporting

Please select the one below that is the best fit for your research. If you are not sure, read the appropriate sections before making your selection.

☒ Life sciences ☐ Behavioural & social sciences ☐ Ecological, evolutionary & environmental sciences

For a reference copy of the document with all sections, see nature.com/documents/nr-reporting-summary-flat.pdf

Life sciences study design

All studies must disclose on these points even when the disclosure is negative.

Sample size	All experiments have been repeated at least three times on independent replicates, and only consistent data are reported. The detection of blebs by CryoEM was performed twice, on independent samples. We did not apply a sample size calculation, since we already have a significant effect with three replicates. In figure 3d, the P value is already very low with only 3 replicates. For Extended Data 8, the difference between the two strains is supported by several significant differences along the Aspect ratio distribution.
Data exclusions	No data were excluded from the analyses.
Replication	All experiments have been repeated at least three times on biologically independent replicates except for the CryoEm images on Fig. 3c and the WB on ED Fig. 5c that were done twice. The WB from ED Fig. 2 and SI Fig. S2 were performed once. All attempts at replications were successful.
Randomization	This is not relevant to our study, biological replicates were generated independently.
Blinding	Blinding was not relevant because the nature of the data did not justify it. Indeed, mass spectrometry analyses, western blots, sequence analysis, image analysis and structure predictions are not subject to blinding because they yield data that you cannot exchange, exagerate or mask. CryoEM images were taken in a collaborating lab that was not aware of the expected phenotypes (but they knew which strain was mutant or wild type). Macrophage infections did not yield significant differences thus blinding was not necessary.

Reporting for specific materials, systems and methods

We require information from authors about some types of materials, experimental systems and methods used in many studies. Here, indicate whether each material, system or method listed is relevant to your study. If you are not sure if a list item applies to your research, read the appropriate section before selecting a response.

Materials & experimental systems

n/a	Involved in the study
☐	☒ Antibodies
☐	☒ Eukaryotic cell lines
☒	☐ Palaeontology
☒	☐ Animals and other organisms
☒	☐ Human research participants
☒	☐ Clinical data

Methods

n/a	Involved in the study
☒	☐ ChIP-seq
☒	☐ Flow cytometry
☒	☐ MRI-based neuroimaging

Antibodies

Antibodies used	The following in-house monoclonal antibodies were used: anti-Omp25 (A59/5F1/C5 and A68/4B10/F5), anti-Omp2b (A63/3H2/B1 and A68/25G5/A5), anti-Lpp. The following in-house polyclonal antibody was used: anti-GcrA (290.S3). The following HRP-couplet secondary antibodies from Dako were used: anti-rabbit Ig (P0217) and anti-mouse Ig (P0260). The following fluorochrome-couplet secondary antibodies from Life Technologies were used: anti-mouse IgG (H+L) Alexa Fluor 488 (A11001) and anti-mouse IgG2a Alexa Fluor 647 (A21241).
Validation	The A59/5F1/C5, A68/4B10/F5 and A68/25G5/A5 monoclonal antibodies specificities were assessed and validated by Cloeckaert et al., 1990 and 1992. The A63/3H2/B1 mnoclonal antibody specificity was assessed and validated by Letesson et al., 1997. The specificity of the A59/5F1/C5 and A63/3H2/B1 monoclonal antibodies was further confirmed following reviewing demands (see SI Fig. S2). For the anti-Lpp serum, it was validated by the absence of a band at the expected size in a Escherichia coli Δlpp mutant compared to a E. coli wild type strain, in extracts enriched for peptidoglycan and peptidoglycan-bound proteins.

Eukaryotic cell lines

Policy information about cell lines

Cell line source(s)	RAW 264.7 murine macrophages cell line were obtained from the ATCC. Low passage count cell (<16) were used for the experiments.
Authentication	RAW 264.7 cells were obtained and authenticated by the ATCC
Mycoplasma contamination	Cell line was not tested for Mycoplasma contamination within our lab
Commonly misidentified lines (See ICLAC register)	RAW 264.7 cell line is not listed as a commonly misidentified cell line